Ultrasmall Monodisperse $NaYF_4$:Yb^{3+}/Tm^{3+} Nanocrystals with Enhanced Near-Infrared to Near-Infrared Upconversion Photoluminescence

Guanying Chen,[†] Tymish Y. Ohulchanskyy,[†] Rajiv Kumar,[†] Hans Ågren,[†,‡] and Prasas N. Prasad[†,*]

[†]Institute for Lasers, Photonics, and Biophotonics, The State University of New York at Buffalo, Buffalo, New York 14260 and [‡]Department of Theoretical Chemistry, Royal Institute of Technology, S-10691 Stockholm, Sweden

ABSTRACT Photoluminescent $NaYF_4$:Yb^{3+}/Tm^{3+} nanocrystals are ideally suited for *in vitro* and *in vivo* photoluminescence (PL) bioimaging due to their virtue of near-infrared to near-infrared (NIR-to-NIR) upconversion (UC); they display PL with a peak at ~800 nm if excited at ~980 nm. Here, we report the synthesis of monodisperse $NaYF_4$:Yb^{3+}/Tm^{3+} nanocrystals of ultrasmall size (7−10 nm) with high UC efficiency. The intensity of their NIR UC emission was demonstrated to increase by up to 43 times along with an increase in the relative content of Yb^{3+} ions from 20 to 100%, with a corresponding decrease in the Y^{3+} content from 80 to 0%. The achieved ultrasmall $NaYbF_4$:2% Tm^{3+} nanocrystals manifest NIR PL emission, which is 3.6 times more intense than that from 25−30 nm sized $NaYF_4$:20% Yb^{3+}/2% Tm^{3+} nanocrystals, previously synthesized and used for *in vitro* and *in vivo* bioimaging. An optimization of both size and UC PL efficiency of NIR-to-NIR nanocrystals provides us with highly efficient optical imaging probes for bioapplications.

KEYWORDS: near-infrared · upconversion photoluminescence · nanocrystals · rare-earth ions

Upconversion (UC) nanocrystals doped with trivalent rare-earth ions (nanophosphors) have shown great potential as optical imaging probes for biomedical applications[1−5] because of their unique merits such as photostability,[6,7] multicolored emissions,[8,9] and, most importantly, ability to display UC emission using low-cost near-infrared (NIR) diode laser.[10] In addition, an efficient UC process can be used for conversion of IR photons in photovoltaics.[11,12] Among UC nanocrystals, the NIR-to-NIR UC nanocrystals of $NaYF_4$:Yb^{3+}/Tm^{3+} are of particular interest,[13,14] not only because $NaYF_4$ has been shown to be the most efficient host material for UC nanocrystals,[15] but also because the excitation at around 975 nm and the photoluminescence (PL) emission peaked at 800 nm are both within the spectral range of 750−1000 nm, which is considered a "window of optical transparency" for biological tissues.[13] This feature allows high contrast *in vitro* and *in vivo* optical bioimaging, as both light attenuation and scattering are significantly reduced in the NIR spectral range and the autofluorescence of cells and tissues is absent under the conditions of UC excitation and emission.[16,17] UC nanocrystals with size larger than 20 nm have been synthesized in both aqueous[18−21] and organic media[22−27] and the synthesized nanocrystals were found to be more monodispersed when the "organic" (e.g., cothermolysis) rather than aqueous method was used.[27] Recent work by our group has shown promising advantages of $NaYF_4$:Yb^{3+}/Tm^{3+} nanocrystals for bioimaging applications *in vitro* and *in vivo*.[13] However, the size of the reported nanophosphors (25−30 nm) is not optimal for their use as bioimaging probes. Body clearance for nanoparticles with size ≤10 nm was shown to be more efficient, allowing the use of higher dose of imaging agents.[28] Despite recent progress in preparing upconversion $NaYF_4$ nanocrystals, synthesis of ultrasmall (with size of less than 10 nm) monodisperse nanocrystals with bright NIR-to-NIR UC emission remains a major challenge as the size of the nanophosphors and the intensity of UC emission are, in general, dependent parameters.[27,29] Because the intensity of emission from rear-earth ions doped in nanophosphors strongly depends on the surrounding crystalline matrix, intensity of UC emission should be generally lower for smaller nanophosphors as they have a higher surface/volume ratio and a larger portion of doped rear-earth ions should be on the surface. Surface passivation (such as surface impurities, ligands, and solvents), which is also higher for smaller nanoparticles, additionally decreases the intensity of the UC PL.[17] It should be noted

*Address correspondence to pnprasad@buffalo.edu.

Received for review March 6, 2010 and accepted May 24, 2010.

Published online May 28, 2010.
10.1021/nn100457j

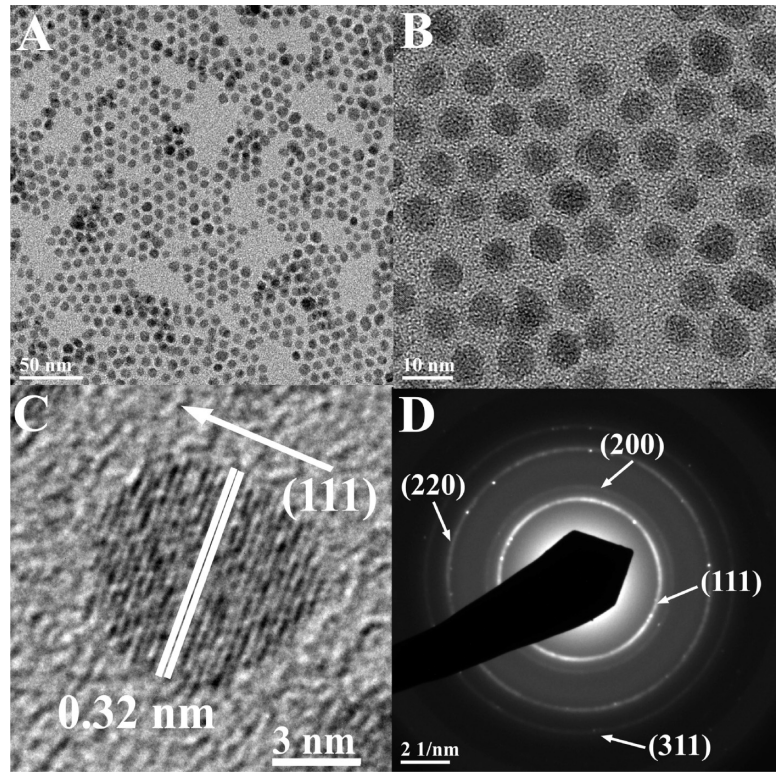

Figure 1. (A,B) TEM images of $NaYF_4$:2% Tm^{3+}/20% Yb^{3+} powders displaying uniformity of the particles. (C) High-resolution TEM image of a single $NaYF_4$:2% Tm^{3+}/20% Yb^{3+} particle, showing lattice fringes. (D) Selected area electron diffraction pattern (SAED) of $NaYF_4$:2% Tm^{3+}/20% Yb^{3+} particles.

that although lithium doping[27,30] and core/shell structure[31] have been employed to increase the visible UC efficiency in nanoparticles by modifying the local crystal structure and by suppressing the energy transfer to surface quenchers, strategies to significantly enhance the intensity of NIR-to-NIR UC emission are scarce in literature.

In this work we present an approach to synthesize ultrasmall (~7 nm) monodisperse nanocrystals of $NaYF_4$:Yb^{3+}/Tm^{3+} displaying UC PL and a simple method to increase NIR-to-NIR UC PL intensity by replacing of Y^{3+} ions in the nanocrystal structure with Yb^{3+} ions. The intensity of the NIR-to-NIR UC PL increased by about 43 times when comparing ultrasmall nanocrystals of $NaYF_4$:20% Yb^{3+}/2% Tm^{3+} and $NaYbF_4$: 2% Tm^{3+}.

RESULTS AND DISCUSSION

Synthesis of Ultrasmall $NaYF_4$:Yb^{3+}/Tm^{3+} Nanocrystals Displaying NIR-to-NIR UC Photoluminescence. Figure 1 shows the transmission electron microscopy (TEM) images of synthesized $NaYF_4$:2% Tm^{3+}/20% Yb^{3+} nanocrystals. As one can see, the synthesized nanoparticles appear nearly spherical in shape and monodisperse. The average diameter of nanoparticles in Figure 1 is around 7.1 nm; this value was confirmed by a detailed analysis of the particle size for ~200 nanoparticles (Supporting Information, Figure S1). In the high-resolution TEM (HR-TEM) image (Figure 1C), the lattice fringes on the individual nanoparticle are clearly distinguished, indicating that the prepared nanoparticles are highly crystalline. The distance between the lattice fringes was measured to be ~0.32 nm, which corresponds to the *d*-spacing for the (111) lattice planes of the cubic $NaYF_4$ structure. Their cubic crystal lattice was also confirmed by selected area electron diffraction (SAED, Figure 1D). The rings of the SAED pattern can be assigned to the (111), (200), (220), and (311) planes of the standard JCPDS 6−0342 cubic $NaYF_4$ structure. The crystallinity of the synthesized nanoparticles was further confirmed by powder X-ray diffraction spectroscopy (XRD).

Figure 2 shows the XRD pattern of the $NaYF_4$:2% Tm^{3+}/20% Yb^{3+} nanocrystals as well as the standard JCPDS 6−0342 cubic structure of $NaYF_4$. It is evident from the intensity of the peaks in Figure 2 that the prepared nanomaterial is highly crystalline in nature. As

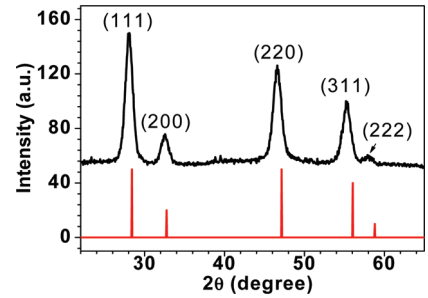

Figure 2. XRD pattern of $NaYF_4$ nanocrystals doped with 2% Tm^{3+}/20% Yb^{3+} ions contrasted with the standard cubic structure of JCPDS 06-0342.

shown in Figure 2, the positions of XRD peaks correspond to the standard JCPDS 6-0342 cubic pattern of $NaYF_4$, and no peaks from other phases or impurities are observed. The XRD peaks have very broad widths originated from the ultrasmall size of nanocrystals. The average crystallite size of the nanocrystals was calculated according to the Scherrer's equation[30]

$$D = K\lambda/\beta \cos\theta \quad (1)$$

where $K = 0.89$, D represents the crystallite size (in nanometers), λ is the wavelength of the Cu Kα radiation, β is the corrected half-width of the diffraction peak, and θ is Bragg's angle of the diffraction peak. According to eq 1 and the half width of the main diffraction peak at 28° in Figure 2, the average size was calculated to be about 7.7 nm, which is in good agreement with TEM results.

The UC PL spectra of colloidal $NaYF_4$ nanocrystals doped with 2% Tm^{3+}/20% Yb^{3+} ions (chloroform suspension) under 975 nm diode laser excitation are shown in Figure 3. Four UC PL bands are clearly resolved; they have maxima at 476, 650, 700, and 802 nm, which correspond to $^1G_4 \rightarrow {}^3H_6$, $^1G_4 \rightarrow {}^3F_4$, $^3F_{2,3} \rightarrow {}^3H_6$, and $^3H_4 \rightarrow {}^3H_6$ transitions of Tm^{3+} ions, respectively.[24] It is also striking that the NIR PL band peaked at 802 nm is much more intense than all the other UC PL bands. The integrated area of this NIR UC PL band is calculated to be about 45 times higher than that of all other UC PL bands, suggesting that radiative deactivation of the upconverted energy predominantly occurs through NIR PL, which is favorable for bioimaging.[32] The inset of Figure 3 shows photographic images of colloidal suspension of $NaYF_4$:Yb^{3+}/Tm^{3+} nanocrystals in chloroform, taken without and with 975 nm excitation (no optical filters were used). As can be seen, the prepared nanocrystals form a transparent and stable colloidal suspension; no precipitation was observed during a period of 1 month. Although the UC PL band with a peak at 802 nm is invisible to the naked eye, a visible blue UC emission in combination with a UC PL spectrum illustrates the NIR PL efficiency. Nevertheless, it is worth noting that because the decrease in size of the nanocrystals results in decreased UC PL, the UC PL efficiency of the synthesized ~7 nm ultrasmall $NaYF_4$:20% Yb^{3+}/2% Tm^{3+} nanocrystals is found to be about 11 times lower than that of 25−30 nm $NaYF_4$:20% Yb^{3+}/2% Tm^{3+} nanocrystals used by us previously as bioimaging probes (see Supporting Information, Figure S2).[13] Therefore, we were exploring ways to increase the efficiency of the NIR UC PL for ultrasmall $NaYF_4$:Yb^{3+}/Tm^{3+} nanocrystals.

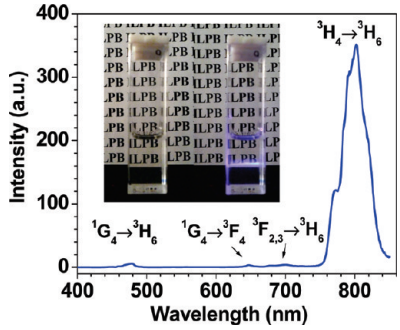

Figure 3. UC PL spectra of colloidal $NaYF_4$ nanocrystals doped with 2% Tm^{3+}/20% Yb^{3+} ions under diode laser excitation at 975 nm. The inset shows photographic images of colloidal $NaYF_4$:Yb^{3+}/Tm^{3+} nanocrystals in chloroform taken without and with laser excitation at 975 nm.

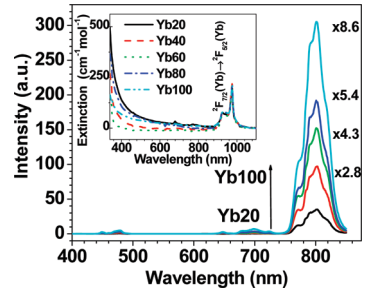

Figure 4. UC PL spectra of colloidal $NaYF_4$ nanocrystals codoped with 2% Tm^{3+} and various concentrations of Yb^{3+} ions (20−100%) under diode laser excitation at 975 nm. The absorbance of all samples has been normalized at 975 nm for the $^2F_{7/2} \rightarrow {}^2F_{5/2}$ transition of Yb^{3+} ions, as shown in the inset.

Enhancement of NIR-to-NIR UC Photoluminescence in Ultrasmall $NaYF_4$:Yb^{3+}/Tm^{3+} Nanocrystals. To increase the efficiency of UC PL, we gradually increased the content of Yb^{3+} ions, replacing the Y^{3+} ions. Figure 4 shows UC PL spectra of colloidal $NaYF_4$ nanocrystals codoped with Tm^{3+} (2%) and various concentrations of Yb^{3+} ions (20, 40, 60, and 100%) when excited by a 975 nm CW diode laser. To allow accurate determination of relative increase in the intensity of the UC PL, absorbance at wavelength corresponding to the $^2F_{7/2} \rightarrow {}^2F_{5/2}$ transition of the Yb^{3+} ions (i.e., where all samples were excited, 975 nm) have been matched to be the same for all samples (Figure 4, inset).[30]

As seen in Figure 4, the UC PL intensity increases by about 2.8, 4.3, 5.4, and 8.6 times when the relative content of Yb^{3+} ions changes from 20% to 40, 60, 80, and 100%, respectively. It is important to note that, because the absorption cross-section for every Yb^{3+}-doped nanocrystal linearly depends on the concentration of the Yb^{3+} ions, the same Yb^{3+} absorption of samples of colloidal nanocrystal suspensions means that the concentration of nanocrystals in these samples is 2, 3, 4, and 5 times lower for nanocrystals containing 40, 60, 80, and 100% of Yb^{3+} ions than the concentration of nanocrystals with 20% of Yb^{3+} ions. Therefore, if the concentrations of the colloidal nanocrystal would be the same, the intensity of UC PL would increase about 5.6, 12.9, 21.6, and 43 times for nanocrystals containing 40, 60, 80, and 100% of Yb^{3+} ions, respectively, if compared to nanocrystals containing 20% of Yb^{3+}. The effect of Tm^{3+} ion concentrations on UC PL was also investigated, but a decrease in UC PL intensity was observed (Supporting Information, Figure S3). All the

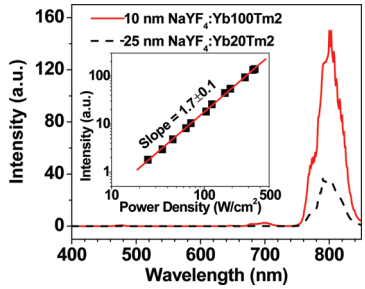

Figure 5. UC PL spectra of ~10 nm $NaYF_4$:100% Yb^{3+}/2% Tm^{3+} nanocrystals and 25−30 nm $NaYF_4$:20% Yb^{3+}/2% Tm^{3+} nanocrystals for the same concentration of nanocrystals. The inset shows the dependence of the intensity of UC emission on the power of excitation at 802 nm of 10 nm $NaYF_4$: 100% Yb^{3+}/2% Tm^{3+} nanocrystals.

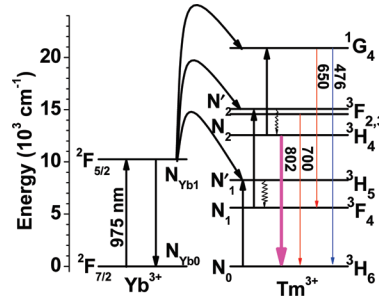

Figure 6. Energy level diagrams of the Yb^{3+} and Tm^{3+} ions and the proposed UC mechanism following diode laser excitation of 975 nm.

nanocrystals of $NaYF_4$:Yb^{3+}/Tm^{3+} are of cubic structure, as shown by SAED, and their average size increases slightly from ~7 to ~10 nm with an increase in the relative content of Yb^{3+} ions from 20 to 100% (Supporting Information, Figures S4 and S5).

Figure 5 contrasts the UC PL spectra of 10 nm nanocrystals of $NaYF_4$:100% Yb^{3+}/2% Tm^{3+} ($NaYbF_4$:2% Tm^{3+}) and 25−30 nm nanocrystals of $NaYF_4$:20% Yb^{3+}/2% Tm^{3+} for samples with the same concentration of nanocrystals. Nanocrystals of $NaYF_4$:20% Yb^{3+}/2% Tm^{3+} (25−30 nm) were prepared following the same protocol described in detail earlier.[13] The average size was also confirmed by TEM (Supporting Information, Figure S6). As one can see in Figure 5, the UC PL intensity of ~10 nm $NaYbF_4$:2% Tm^{3+} nanocrystals is about 3.6 times higher than that of the 25−30 nm $NaYF_4$:20% Yb^{3+}/2% Tm^{3+} nanocrystals, which have already been used in *in vivo* and *in vitro* bioimaging.[13] This result shows that the NIR-to-NIR UC PL intensity of the prepared ultrasmall nanocrystals $NaYF_4$:Yb^{3+}/Tm^{3+} is sufficient enough to be used for *in vivo* and *in vitro* bioimaging. We have also recorded decays of NIR PL peaked at 802 nm for 25−30 nm $NaYF_4$:20% Yb^{3+}/2% Tm^{3+} nanocrystals and 7−10 nm nanocrystals of $NaYF_4$: 20−100% Yb^{3+}, 2% Tm^{3+}; PL lifetime was determined to be in the range of 35−60 μs (Supporting Information, Figure S7).

The inset of Figure 5 shows the dependence of UC PL from ~10 nm $NaYbF_4$:2% Tm^{3+} nanocrystals on the power of excitation. In general, the number of photons which are required to populate the upper emitting state under unsaturated condition can be obtained by the relation[15]

$$I_f \propto P^n \qquad (2)$$

where I_f is the photoluminescence intensity, P is the pump laser power, and n is the number of the laser photons required. As can be seen in the inset of Figure 5, a slope value of 1.7 was observed, illustrating that two-photon processes were involved to generate the NIR-to-NIR UC PL with peak at 802 nm.

Mechanism for NIR-to-NIR UC Photoluminescence Enhancement. Figure 6 shows the energy levels of the involved Yb^{3+} and Tm^{3+} ions as well as the proposed UC pathways under excitation with 975 nm diode laser.[33] The corresponding photons can only excite the Yb^{3+} ions, because the Tm^{3+} ions have no such excited energy level above the ground state. As shown in Figure 6, the first energy transfer process from the Yb^{3+} to the Tm^{3+} ion excites the $^3H_6$ to the $^3H_5$ state with the redundant energy dissipated by phonons. Subsequently, the Tm^{3+} ion relaxes nonradiatively to the lower $^3F_4$ state and further populates the $^3F_{2,3}$ state through a second energy transfer process from the Yb^{3+} to the Tm^{3+} ion. The weak UC PL with maximum at 700 nm is associated with the radiative transition from the $^3F_{2,3}$ state to the ground state. Additionally, the strong NIR PL with peak at 802 nm arises from the $^3H_4 \rightarrow {}^3H_6$ transition, where the $^3H_4$ state is populated by the efficient nonradiative relaxation from the $^3F_{2,3}$ state. The third energy transfer process from the Yb^{3+} to the Tm^{3+} ion excites the $^3H_4$ to the $^1G_4$ state from which the UC PL peaked at 476 and 650 nm is generated, which corresponds to the $^1G_4 \rightarrow {}^3H_6$ and $^1G_4 \rightarrow {}^3F_4$ transitions, respectively.

To verify the proposed UC mechanism and interpret an enhancement of the NIR UC PL, we utilized the following steady-state equations:

$$W_0 N_0 N_{Yb1} - R_1' N_1' - \beta_1 N_1' = 0 \qquad (3.1)$$

$$\beta_1 N_1' - W_1 N_1 N_{Yb1} - R_1 N_1 = 0 \qquad (3.2)$$

$$W_1 N_1 N_{Yb1} - \beta_2 N_2' - R_2' N_2' = 0 \qquad (3.3)$$

$$\beta_2 N_2' - R_2 N_2 = 0 \qquad (3.4)$$

$$N_{Yb1} = \rho\sigma N_{Yb0} \qquad (3.5)$$

where N_0, N_1, N_1', N_2, and N_2' are the population densities of the $^3H_6$, $^3F_4$, $^3H_5$, $^3H_4$, and $^3F_{2,3}$ states of the Tm^{3+} ions; R_1, R_1', R_2, and R_2' are the radiative rates of the $^3F_4$, $^3H_5$, $^3H_4$, and $^3F_{2,3}$ states of the Tm^{3+} ions; W_0 and W_1 are the rates of the energy transfer from the excited Yb^{3+} ions to the $^3H_6$ and $^3F_4$ states of Tm^{3+} ions; N_{Yb0} and N_{Yb1} are the population densities of the Yb^{3+} ions in the ground and the excited states, respectively; β_1 and β_2 are nonradiative decay rates of $^3H_5$ and $^3F_{2,3}$ states, re-

spectively; ρ is the laser photon number density; and σ denotes the absorption cross-section of the Yb^{3+} ion, while R is the radiation rate of the $^2F_{5/2}$(Yb) state. Equation 3.5 is the result of an approximation obtained in ref 34.

In the following discussion, the parameters R_1' in eq 3.1 and R_2' in eq 3.3 are omitted, because the radiative rates from $^3H_5$ and $^3F_{2,3}$ states have been known to be much less than their nonradiative rates. Additionally, the radiative decay rate at the $^3F_4$ state, that is, R_1, is supposed to be much higher than its UC rate, that is, W_1N_{Yb1}.[34] Thus, from eqs 3.1−3.5, we can obtain the population and the PL intensity of the NIR-emitting $^3H_4$ state

$$N_2 = \frac{W_0W_1N_0}{R_1R_2}\sigma^2N_{Yb0}^2\rho^2 \quad (4.1)$$

$$I_f = N_2h\nu_{NIR}R_2 = \frac{W_0W_1N_0}{R_1}h\nu_{NIR}\sigma^2N_{Yb0}^2\rho^2 \quad (4.2)$$

where I_f is the intensity of NIR UC PL, h is Plank constant, and ν_{NIR} is the frequency of NIR emission. From eq 4.2, the efficiency of NIR UC (UCE) for absorption-normalized solution can be obtained:

$$\mathrm{UCE(Yb)} = \frac{I_f}{\sigma\rho N_{Yb0}} = \frac{N_0}{R_1}\sigma\rho W_0(\mathrm{Yb})W_1(\mathrm{Yb})N_{Yb0} \quad (5)$$

As follows from eq 4.2, the intensity of NIR UC photoluminescence should have a quadratic dependence on the power of excitation, which is in good agreement with experimental observations in Figure 5. Because the concentration of Tm^{3+} ions is constant and the same excitation power is employed for all the samples, UCE(Yb) only depends on $W_0(\mathrm{Yb})W_1(\mathrm{Yb})N_{Yb0}$. According to eq 5, the increase in Yb^{3+} ions should lead to at least 2, 3, 4, and 5 times higher UC efficiency in nanocrystals $NaYF_4$ for Yb^{3+} ions of 40, 60, 80, and 100%, which is in general agreement with the experimental result shown Figure 4. A slight deviation between the theoretical data and the experimental observation might arise from the fact that the energy transfer efficiency, that is, the parameters of W_0(Yb) and W_1(Yb), also increases with the increase in number of Yb^{3+} per Tm^{3+} ion and a corresponding decrease in an average distance between Yb^{3+} and Tm^{3+} ions.[10]

SUMMARY

In conclusion, we have developed a method to synthesize monodispersed, 7−10 nm sized $NaYF_4$:Yb^{3+}/Tm^{3+} nanocrystals. Their NIR-to-NIR UC photoluminescence intensity was shown to increase about 8.6 times per Yb^{3+} concentration and 43 times per nanoparticle, with an increase in relative content of the doped Yb^{3+} ions from 20 to 100%. Such enhancement arises from the increased absorptions induced by the Yb^{3+} ions and the increased efficiency of energy transfer between the Yb^{3+} and Tm^{3+} ions. The achieved ultrasmall NIR-to-NIR $NaYbF_4$:2% Tm^{3+} nanocrystals manifest NIR UC PL with intensity 3.6 times higher (per nanoparticle) than the 25−30 nm nanocrystals of $NaYF_4$:20% Yb^{3+}/2% Tm^{3+} that have been previously used as *in vitro* and *in vivo* bioimaging probes. This work constitutes a promising step to deploy $NaYF_4$:Yb^{3+}/Tm^{3+} nanocrystals as optimal NIR-to-NIR UC PL imaging probes.

METHODS

Synthesis of Nanocrystals $NaYF_4$:Yb^{3+}/Tm^{3+}. Nanocrystals $NaYF_4$ doped with 2% Tm^{3+} and 20, 40, 60, 80, and 100% Yb^{3+} were synthesized using a modified cothermolysis method. All chemicals used in the synthesis were purchased from Sigma-Aldrich and used as received. Aliquots of 1 mmol lanthanide oxides (Tm_2O_3, Yb_2O_3, and Y_2O_3) and 2 mmol NaOH were mixed and dissolved in 50% concentrated trifluoroacetic acid at 95 °C in a three-necked 100 mL flask. The molar compositions of the feed solution were [Na/(Tm + Yb + Y)] = 1, Tm/(Tm + Yb + Y)] = 0.02, and [Yb/(Tm + Yb + Y)] = 0.18, 0.38, 0.58, 0.78, and 0.98 for nanocrystals $NaYF_4$ doped with 2% Tm^{3+} and 20, 40, 60, 80, and 100% Yb^{3+}, respectively. Then, the solutions were evaporated to dryness under an argon gas purge. Next, 16 mL of oleic acid (90%, technical grade) and 8 mL of oleylamine (70%, technical grade) were added into the three-necked flask. The resulting solution was then heated at 120 °C with magnetic stirring for 30 min to remove water and oxygen. The solution was then heated to 275 °C at a rate of about 12 °C per min under argon gas protection and kept at this temperature under vigorous stirring for about 0.5 h. A needle was used to let the argon gas out during the synthesis. The mixture was cooled to room temperature and precipitated by acetone in an ultrasonic bath and collected by centrifugation at 11000 rpm for 12 min. The precipitate was washed with ethanol several times, and the nanocrystals were dispersed in 8 mL of chloroform for further characterizations.

Instruments. The size and morphology of the nanocrystals were characterized by transmission electron microscopy (TEM) using a JEM-2010 microscope at an acceleration voltage of 200 KV. The powder X-ray diffraction (XRD) patterns were recorded by a Siemens D500 diffractometer using Cu Kα radiation (λ = 0.15418 nm). The 2θ angle of the XRD spectra was recorded at a scanning rate of 5°/minute. Absorption spectra of transparent colloidal nanocrystals were acquired using a Shimadzu UV−visible-NIR scanning spectrophotometer. UC PL spectra were recorded using a Fluorolog-3.11 Jobin Yvon spectrofluorometer with a slit width defining spectral resolution of 1 nm. The PL was excited at 975 nm using a fiber-coupled laser diode (Q-Photonics). All UC PL spectra have been corrected for the spectral sensitivity of the system. Photographic images of UC nanocrystals colloidal were taken by a digital camera (Lumix DMC-Fx520, Japan) without adding any filter.

Acknowledgment. This work was supported by grants from the National Institutes of Health (R01CA119358 and RO1CA104492), the Swedish Energy Agency (project 32076-1), and the John R. Oishei Foundation.

Supporting Information Available: Histogram of nanocrystal size distribution, comparison of the UC PL efficiency for 7 and 25 nm nanocrystals $NaYF_4$:20% Yb^{3+}/2% Tm^{3+}; comparison of the UC PL efficiency for 10 nm $NaYF_4$ doped with 100% Yb^{3+} and various Tm^{3+} ions, TEM images, and histograms of size distribu-

tion for ultrasmall nanocrystals $NaYF_4$ doped with 2% of Tm^{3+} and 20−100% of Yb^{3+} ions; TEM images of 25−30 nm $NaYF_4$: 20% Yb^{3+}/2% Tm^{3+} nanocrystals, decay profiles of NIR PL at 802 nm for 25−30 nm $NaYF_4$:20% Yb^{3+}/2% Tm^{3+} nanocrystals, and 7−10 nm $NaYF_4$:20%−100% Yb^{3+}/2% Tm^{3+} nanocrystals. This material is available free of charge *via* the Internet at http://pubs.acs.org.

REFERENCES AND NOTES

1. Prasad, P. N. *Introduction to Biophotonics*; Wiley-Interscience: New York, 2003; pp 534−535.
2. Rijke, F.; Zijlmans, H.; Li, S.; Vail, T.; Rapp, A. K.; Niedbala, R. S.; Tanke, H. J. Upconverting phosphor reporters for nucleic acid microarrays. *Nat. Biotechnol.* **2001**, *19*, 273–276.
3. Zhang, P.; Steelant, P.; Kumar, M.; Scholfield, M. Versatile photodynamic therapy at infrared excitation. *J. Am. Chem. Soc.* **2007**, *129*, 4526–4527.
4. Chatterjee, D. K.; Rufaihah, A. J.; Zhang, Y. Upconversion fluorescence imaging of cells and small animals using lanthanide doped nanocrystals. *Biomaterials* **2008**, *29*, 937–943.
5. Xiong, L. Q.; Chen, Z. G.; Yu, M. X.; Li, F. Y.; Liu, C.; Huang, C. H. Synthesis, characterization, and *in vivo* targeted imaging of amine-functionalized rare-earth upconverting nanophosphors. *Biomaterials* **2009**, *30*, 5592–5600.
6. Park, Y.; Kim, J. H.; Lee, K. T.; Jeon, K. S.; Na, H. B.; Yu, J. H; Kim, H. M.; Lee, N.; Choi, S. H.; Baik, S.; Kim, H.; Park, S. P.; Park, B.; King, Y. W.; Lee, S. H.; Yong, S. Y.; Song, I. C.; Moon, W. K.; Suh, Y. D.; Hyeon, T. Nonblinking and nonbleaching upconverting nanoparticles as an optical imaging nanoprobe and T1 magnetic resonance imaging contrast agent. *Adv. Mater.* **2009**, *21*, 4467–4471.
7. Wu, S. W.; Han, G.; Milliron, D. J.; Aloni, S.; Altoe, V.; Talapin, D. V.; Cohen, B. E.; Schuck, P. J. Non-blinking and photostable upconverted luminescence from single lanthanide-doped nanocrystals. *Proc. Natl. Acad. Sci. U.S.A.* **2009**, *106*, 10917–10921.
8. Heer, S.; Kömpe, K.; Güdel, H. U.; Haase, M. Highly efficient multicolour upconversion emission in transparent colloids of lanthanide-doped $NaYF_4$ nanocrystals. *Adv. Mater.* **2004**, *16*, 2102–2105.
9. Wang, F.; Liu, X. G. Upconversion multicolor rine-tuning: Visible to near-infrared emission from lanthanide-doped $NaYF_4$ nanocrystals. *J. Am. Chem. Soc.* **2008**, *130*, 5642–5643.
10. Auzel, F. Upconversion and anti-stokes processes with f and d ions in solids. *Chem. Rev.* **2004**, *104*, 139–174.
11. Shalav, A.; Richards, R. S.; Trupke, T.; Krämer, K. W.; Güdel, H. U. Application of $NaYF_4$:Er^{3+} upconverting phosphors for enhanced near-infrared silicon solar cell response. *Appl. Phys. Lett.* **2005**, *86*, 013505.
12. Ende, M.; Aarts, L.; Meijerink, A. Lanthanide ions as spectral converters for solar cells. *Phys. Chem. Chem. Phys.* **2009**, *11*, 11081–11095.
13. Nyk, M.; Kumar, R.; Ohulchanskyy, T. Y.; Bergey, E. J.; Prasad, P. N. High contrast *in vitro* and *in vivo* photoluminescence bioimaging using near infrared to near infrared upconversion in Tm^{3+} and Yb^{3+} doped fluoride nanophosphors. *Nano Lett.* **2008**, *8*, 3834–3838.
14. Xu, C.; Svensson, N.; Axelsson, J.; Svenmaker, P.; Somesfalean, G.; Chen, G. Y.; Liang, H. J.; Liu, H. C.; Zhang, Z. G.; Andersson-Engels, S. Autofluorescence insensitive imaging using upconverting nanocrystals in scattering media. *Appl. Phys. Lett.* **2008**, *93*, 171103.
15. Chen, G. Y.; Liu, H. C. ; Somesfalean, Gabriel; Liang, H. J.; Zhang, Z. G. Upconversion emission tuning from green to red in Yb^{3+}/Ho^{3+}-codoped $NaYF_4$ nanocrystals by tridoping with Ce^{3+} ions. *Nanotechnology* **2009**, *20*, 385704.
16. Kumar, R.; Nyk, M.; Ohulchanskyy, T. Y.; Flask, C. A.; Prasad, P. N. Combined optical and MR bioimaging using rare earth ion doped $NaYF_4$ nanocrystals. *Adv. Funct. Mater.* **2009**, *19*, 853–859.
17. Wang, F.; Liu, X. G. Recent advances in the chemistry of lanthanide-doped upconversion nanocrystals. *Chem. Soc. Rev.* **2009**, *38*, 976–989.
18. Zeng, J. H.; Su, J.; Li, Z. H.; Yan, R. X.; Li, Y. D. Synthesis and upconversion luminescence of hexagnonal-phase $NaYF_4$:Yb, Er^{3+} phosphors of controlled size and morphology. *Adv. Mater.* **2005**, *17*, 2119–2123.
19. Liu, X. M.; Zhao, J. W.; Sun, Y. J.; Song, K.; Yu, Y.; Du, H.; Kong, X. G.; Zhang, H. Ionothermal synthesis of hexagonal-phase $NaYF_4$:Yb^{3+}, Er^{3+}/Tm^{3+} upconversion nanophosphors. *Chem. Commun.* **2009**, 6628–6630.
20. Ghosh, P.; Patra, A. Tuning of crystal phase and luminescence properties of Eu^{3+} doped sodium yttrium fluoride nanocrystals. *J. Phys. Chem. C* **2008**, *112*, 3223–3231.
21. Yi, G. S.; Lu, H. C.; Zhao, S. Y.; Ge, Y.; Yang, W. J.; Chen, D. P.; Guo, L. H. Synthesis, characterization, and biological applications of size-controlled nanocrystalline $NaYF_4$:Yb, Er infrared-to-visible upconversion phosphors. *Nano Lett.* **2004**, *4*, 2191–2196.
22. Mai, H. X.; Zhang, Y. W.; Si, R.; Yan, Z. G.; Sun, L. D.; You, L. P.; Yan, C. H. High-quality sodium rare-earth fluoride nanocrystals: Controlled synthesis and optical properties. *J. Am. Chem. Soc.* **2006**, *128*, 6426–6436.
23. Li, Z. Q.; Zhang, Y. An efficient and user-friendly method for the synthesis of hexagonal-phase $NaYF_4$:Yb, Er/Tm nanocrystals with controllable shape and upconversion fluorescence. *Nanotechnology* **2008**, *19*, 345606.
24. Boyer, J. C.; Cuccia, L. A.; Capobianco, J. A. Synthesis of colloidal upconverting $NaYF_4$:Er^{3+}/Yb^{3+} and Tm^{3+}/Yb^{3+} monodisperse nanocrystals. *Nano Lett.* **2007**, *7*, 847–852.
25. Shan, J. N.; Ju, Y. G. Controlled synthesis of lanthanide-doped $NaYF_4$ upconversion nanocrystals *via* ligand induced crystal phase transition and silica coating. *Appl. Phys. Lett.* **2007**, *91*, 123103.
26. Ehlert, O.; Thomann, R.; Darbandi, M.; Nann, T. A four-color colloidal multiplexing nanoparticle system. *ACS Nano* **2008**, *2*, 120–124.
27. Wang, H. Q.; Nann, T. Monodisperse upconverting nanocrystals by microwave-assisted synthesis. *ACS Nano* **2009**, *3*, 3804–3808.
28. Longmire, M.; Choyke, P. L.; Kobayashi, H. Clearance properties of nano-sized particles and molecules as imaging agents: considerations and caveats. *Nanomedicine* **2008**, *3*, 703–717.
29. Yi, G. S.; Chow, G. M. Synthesis of hexagonal-phase $NaYF_4$: Yb, Er and $NaYF_4$:Yb, Tm nanocrystals with efficient upconversion fluorescence. *Adv. Funct. Mater.* **2006**, *16*, 2324–2329.
30. Chen, G. Y.; Liu, H. C.; Liang, H. J.; Somesfalean, G.; Zhang, Z. G. Upconversion emission enhancement in Yb^{3+}/Er^{3+}-codoped Y_2O_3 nanocrystals by tridoping with Li^+ ions. *J. Phys. Chem. C* **2008**, *112*, 12030–12036.
31. Vetrone, F.; Naccache, R.; Mahalingam, V.; Morgan, C. G.; Capobianco, J. A. The active-core/active-shell approach: A strategy to enhance the upconversion luminescence in lanthanide-doped nanoparticles. *Adv. Funct. Mater.* **2009**, *19*, 2924–2929.
32. Chen, G. Y.; Zhang, Y. G.; Somesfalean, G.; Zhang, Z. G. Two-color upconversion in rare-earth-ion-doped ZrO_2 nanocrystals. *Appl. Phys. Lett.* **2006**, *89*, 163105.
33. Gruber, J. B.; Hills, M. E.; Macfarlane, R. M.; Morrison, C. A.; Turner, G. A.; Quarles, G. J.; Kintz, G. J.; Esterowitz, L. Spectra and energy levels in Tm^{3+}:$Y_3Al_5O_{12}$. *Phys. Rev. B* **1989**, *40*, 9464–9478.
34. Pollnau, M.; Gamelin, D. R.; Lüthi, S. R.; Güdel, H. U.; Hehlen, M. P. Power dependence of upconversion luminescence in lanthanide and transition-metal-ion systems. *Phys. Rev. B* **2000**, *61*, 3337–3346.